WIRELESS COMMUNICATIONS AND MOBILE COMPUTING
Wirel. Commun. Mob. Comput. 2002; **2**:719–733 (DOI: 10.1002/wcm.89)

Space–time receivers for GSM radio interfaces in subway tunnel environments

Miguel González-López, Adriana Dapena and Luis Castedo*,†

Departamento de Electrónica y Sistemas,
Universidad de A Coruña,
Facultad de Informática,
Campus de Elviña, A Coruña,
Spain

Martine Lienard and Pierre Degauque

Université de Lille,
Dept. Electronique,
Bat. P3,
59655 Villeneuve d'Ascq cedex
France

María J. Asarta and Pedro Crespo

Centro de Estudios e Investigaciones
Técnicas de Guipuzcoa (CEIT)
Paseo de Manuel Lardizábal, 15,
20018 San Sebastián,
Spain

Summary

In this paper, we investigate how to increase the capacity of GSM (Global System for Mobile communications) radio interfaces in subway tunnel environments by means of antenna arrays and Space–Time (ST) receivers. We address the modeling, both theoretically and experimentally, of the multiple-antenna wireless channels encountered in subway tunnels. We demonstrate that propagation is conveniently modeled by a flat-fading channel, but there exist strong spatial correlations among channel components that decrease capacity and affect receivers' performance. Different space–time GSM receiving strategies have also been investigated. We first consider ST equalization techniques that only account for the noise and the controlled Intersymbol Interference (ISI) introduced by the modulation format employed in GSM. Then, we analyze the performance of receivers that incorporate ST coding capabilities and show the superior performance of iterative MAP (*Maximum a Posteriori*) receivers that interchange soft information among the equalizer and the ST decoder. All receivers are evaluated with experimental channels measured in the subway of Paris. Copyright © 2002 John Wiley & Sons, Ltd.

KEY WORDS

space–time receivers
GSM radio interfaces
Multiple-Input Multiple-Output (MIMO) channels
iterative *Maximum a Posteriori* (MAP) decoding

*Correspondence to: Luis Castedo, Departamento de Electrónica y Sistemas, Universidad de A Coruña, Facultad de Informática, Campus de Elviña, A Coruña, Spain.
†E-mail: luis@udc.es
Contract/grant sponsor: European Commission; contract/grant number: IST-1999-20006 (ESCORT project).

1. Introduction

GSM is undoubtedly the most successful second-generation digital mobile radio system. Since it has been sponsored by the European telecommunication industry, a large number of European companies dominate the technologies related with GSM radio transmission. As a consequence, the GSM radio interface (GSM-R) has been also adopted in 1993 by the standardized digital radio system available for the European railway networks and a specific frequency band, called the *R band* (876–880 MHz 921–925 MHz), has been reserved for them. Because of the conservative nature of its market, it is expected that railway radio communication systems will employ GSM-R for the long-term future.

It is very likely that urban transport operators (typically metro operators) adopt a digital radio system similar to that used in conventional railway transportation. In urban transportation systems, however, requirements for radio communications are more stringent, and it is highly desirable to offer phone and video services for either security or entertainment. These increasing needs for communication imply the availability of a high data rate and a high-quality wireless access over fading channels at almost wireline quality. In this paper, we investigate the use of multiple antennas at the transmit and receive sides in combination with signal processing and coding as a promising means to meet all these requirements.

Recent information theory investigations have demonstrated that the capacity of wireless channels can be considerably increased, at no extra bandwidth or power consumption, if the multipath is sufficiently rich and properly exploited by means of multielement antennas at both transmission and reception [1,2,3]. The basic idea is to approach the transmission through multipath channels from a new perspective in which multipath signal propagation is no longer viewed as an impairment but as a phenomenon that provides spatial diversity that can be successfully exploited to improve reception. Multipath propagation enables the existence of multiple spatial parallel data pipes that allow the spatial multiplexing of several data streams and, thus, the possibility of increasing channel capacity with the number of antennas.

Spatial diversity can be successfully exploited by means of specific signal processing techniques suitable for multiple transmitting and receiving antennas. An overview of the most relevant existing ST signal processing schemes can be found in Reference [4]. The performance of these techniques can be substantially improved by including codes specifically designed to take into account both the spatial and temporal dimensions [5]. These techniques are collectively known as Space–Time Coding (STC) and for a tutorial review of them the reader is referred to Reference [6] and references therein. In this paper we will investigate how to use STC to increase the capacity of GSM radio interfaces in subway tunnel environments. To our knowledge no work has been done on this specific topic. Existing works on STC have been mainly devoted to outdoors and Small Office/HOme (SOHO) environments, and advanced third-generation mobile communication technologies [7].

GSM radio interfaces impose the specific constraint that the modulation format to be used should be Gaussian Minimum Shift Keying (GMSK) and thus, certain controlled ISI is deliberately introduced at transmission. This means that the coder/modulator stages can be interpreted as a concatenated code that can be very efficiently decoded using iterative (turbo) ST decoding strategies. The design of ST turbo codes have been investigated by several authors [8,9,10,11]. In this work, however, we will not address the problem of coding design. Instead, we will assume that the outer encoder is a conventional ST convolutional encoder, and we will investigate the advantages of using an iterative approach to combine the equalization and decoding stages.

Channel modeling is an important issue when designing ST communication systems. In subway scenarios, radio propagation is severely affected by numerous reflections on the walls and ceilings of tunnels and stations. In this paper we demonstrate, both theoretically and experimentally, that the relative delays between these reflections are negligible when compared to the symbol rate used in GSM systems. As a consequence, wireless channels are appropriately modeled as flat-fading channels. In addition, it is common practice to assume that spatial correlation among multipath components is low and model channels as spatially uncorrelated fading channels. Experimental measurements reveal, however, that this is not the case in subway environments in which, due to the geometrical characteristics of the tunnels, there exist strong spatial correlations that severely affect channel capacity [12]. These strong spatial correlations will also have an enormous impact on the performance of ST receivers.

The remainder of this paper is organized as follows: We describe the signal model of a GSM wireless communication system with spatial diversity in Section 2.

Section 3 is devoted to channel modeling, whereas Section 4 is dedicated to ST equalizers that do not take into account the redundancy induced by the ST encoder in transmission. These receivers only combat the noise and the controlled ISI introduced by the modulation format used in GSM. Receivers that consider the ST encoder at transmission are examined in Section 5 in which both iterative and noniterative MAP decoding strategies are considered. Finally, Section 6 ends the paper with the conclusions.

2. Signal Model

Let us consider the block diagram of a GSM wireless communication system with ST coding depicted in Figure 1. The original bit sequence $u(n)$ is encoded with a ST encoder to produce a vector of symbols $\mathbf{c}(n) = [c_1(n), \ldots, c_N(n)]^T$ (N is the number of transmitting antennas) with a certain spatiotemporal correlation structure. These symbols are subsequently interleaved, resulting in the sequence $\mathbf{b}(n)$ and modulated using the GMSK modulation format. The transmitted symbols $\mathbf{s}(n) = s_1(n), \ldots, s_N(n)$ are then up-converted to produce the analog signal radiated through the antennas. Multipath propagation occurs between each transmitting and receiving element resulting in a Multiple Input Multiple Output (MIMO) channel. A bank of $L \times 1$ matched filters is employed at the receiver to obtain a set of sufficient statistics $\mathbf{x}(n) = [x_1(n), x_2(n), \ldots, x_L(n)]^T$. The goal in ST decoding is to detect the original sequence $u(n)$ from the observations $\mathbf{x}(n)$. Toward this aim we propose a two-stage decoding scheme. The first stage is an ST equalizer that compensates the effect of both the noise and the controlled ISI induced by the GMSK modulation format. Perfect Channel State Information (CSI) is assumed in this equalizing stage although in practical implementations this information would be supplied by a channel estimation step. The second stage is a ST decoder that undoes the channel encoding introduced at transmission.

Let us further elaborate the signal model. GMSK is a partial response Continuous Phase Modulation (CPM) with fixed modulation index $h = 0.5$. The performance analysis of GMSK systems is difficult because GMSK is a nonlinear modulation format. Nevertheless, it can be approximated by a partial response PAM signal that can be analyzed more easily. Indeed, CPM signals can be expressed by a Laurent expansion [13] that consists of the sum of 2^{m-1} PAM signals where m is the memory of the modulation ($m = 3$ in GSM). It can be demonstrated that the first PAM component contains 99.63% of the total GMSK signal energy. As a consequence, the GMSK signal radiated by the ith transmitting antenna for a GSM frame of K bits, $s_i(t; \mathbf{b}_i(0\colon K-1))$, can be accurately approximated by the following expression

$$s_i(t; \mathbf{b}_i(0\colon K-1)) \approx \sqrt{\frac{2E_b}{T}} \sum_{n=0}^{K-1} a_i(n)\, p(t - nT) \tag{1}$$

where $\mathbf{b}_i(0\colon K-1) = [b_i(0) b_i(1) \cdots b_i(K-1)]^T$ is the binary information bearing sequence, E_b is the bit energy, T is the symbol period, $a_i(n) = j\, a_i(n-1) b_i(n)$ are the transmitted symbols and $p(t)$ is a partial response pulse waveform that expands along the interval $[0, mT]$. It is important to note that the transmitted symbols belong to a Quadrature Phase Shift Keying (QPSK) constellation (i.e. $a_i(n) \in$

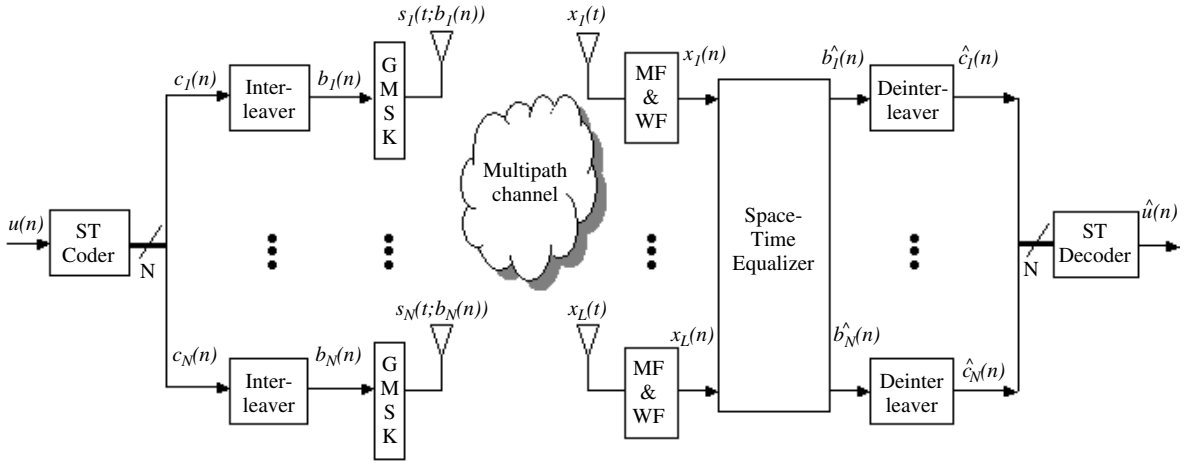

Fig. 1. Block diagram of a GSM wireless communication system.

$\{1, j, -1, -j\}$), are uncorrelated and have unit variance [13]. We assume that differential precoding is employed before the modulator, so $a_i(n) = j^n b_i(n)$.

The transmitted signals arrive at an array of L receiving antennas and thus we can model the propagation channel as a $N \times L$ MIMO system. As it is explained in the following section, multipath propagation introduces a negligible amount of time dispersion in subway tunnel environments and, thus, the wireless channel can be modeled as flat-fading. In this case, the received signal in the jth receiving antenna can be expressed as follows:

$$x_j(t) = \sum_{i=1}^{N} h_{ji} s_i(t; \mathbf{b}_i(0{:}\, K-1)) + n_j(t), \quad j = 1, \ldots, L \tag{2}$$

where h_{ji} is the channel impulse response that models the fading corresponding to the subchannel between the ith transmitting antenna and the jth receiving antenna. The noise component $n_j(t)$ is modeled as a continuous-time white Gaussian random process.

In order to detect the transmitted symbols, the signals $x_j(t)$, $j = 1, \ldots, L$ are passed through a bank of filters matched to the impulse response of the modulation pulse, $p(t)$, and sampled at the symbol rate to produce a set of sufficient statistics [14]. It is important to note that the noise at the output of the matched filters is colored because $p(t)$ does not satisfy the zero-ISI condition. In order to simplify the mathematical derivations, it is highly desirable to handle observations contaminated with white noise and thus a discrete-time Whitening Filter (WF) is placed after each Matched Filter (MF) [15]. In order to eliminate the rotation introduced by the GMSK modulation, we multiply the available observations by j^{-n}, resulting in a set of observations of the form

$$\begin{aligned} x_j(n) &= \sum_{i=1}^{N} h_{ji} \sum_{l=0}^{m-1} f(l) b_i(n-l) + g_j(n) \\ &= \sum_{i=1}^{N} h_{ji} s_i(n) + g_j(n) \end{aligned} \tag{3}$$

where $g_j(n)$ is a discrete-time white Gaussian noise, m is the memory of the modulation ($m = 3$ in GSM) and $f(l) = [0.8053, 0.5853, 0.0704]$ is the equivalent discrete-time impulse response that takes into account the transmitting, receiving and whitening filters. Finally, vector notation can be used to write the observations in a more compact way as follows:

$$\mathbf{x}(n) = \mathbf{H}\mathbf{s}(n) + \mathbf{g}(n) \tag{4}$$

This is the vector that will be processed to detect the original sequence $u(n)$.

3. Channel Modeling

This section deals with the theoretical and experimental modeling of the propagation in tunnels when multiple antennas are used at both transmission and reception. We will start by applying the image theory to determine the delay spread and coherence bandwidth of a straight tunnel with a rectangular cross section when a single antenna is used at both transmission and reception. Next, we will explain the experimental measurements that have been carried out in the subway of Paris with four transmitting and four receiving antennas. These experiments corroborate that the channel delay spread is negligible when compared to the GSM symbol period. In addition, statistical analysis carried out on the obtained measurements reveal the existence of strong spatial correlations that diminish the channel capacity with respect to an uncorrelated Rayleigh-fading channel.

3.1. Single-Antenna Theoretical Modeling

Image theory is the most widely used method to model the propagation of high-frequency waves in complex environments. Although its principle is quite simple, it nevertheless assumes that all possible paths linking the transmitting and the receiving antennas can be determined. These paths can be easily obtained if the tunnel is straight and has a rectangular section. This assumption will be made in order to obtain a first approximation of the single-antenna channel characteristics in subway environments. If the tunnel is arched and/or curved, more accurate models have to be considered that make use of diverse ray-launching techniques such as those proposed in References [16] and [17]. These methods, however, are difficult to implement, and the computational time may become prohibitive for a wide-band analysis in long tunnels.

The application of the image-theory principle to model the propagation in tunnels was originally described by Mahmoud and Wait [18]. This work has been subsequently extended to consider many different applications such as mines, roads and railways in References [19] and [20]. In the sequel, we emphasize the main theoretical results that may have an impact on the measurement procedure.

Let us consider a rectangular tunnel 7 m high where one transmitting and one receiving half-wave

antennas are put at a height of 2 m and located at a distance of 1 m and 6 m from the tunnel wall, respectively. Figure 2 plots the variation of the coherence bandwidth, B_c, *versus* the tunnel width at a distance from the transmitter of 300 m obtained with conventional image theory techniques. The equivalent conductivity of the walls is $\sigma = 10^{-2}$ S m^{-1} and the relative permittivity ε_r has been chosen to be equal to 5. Nevertheless, it must be noted that parametric studies show that neither the position of the antennas inside the tunnel nor the electrical characteristics of the walls are critical.

Figure 2 also plots the regression line that approximates the obtained results. It is apparent that B_c is a decreasing function of the tunnel width. For instance, in a large tunnel 15 m wide, a coherence bandwidth of 20 MHz is obtained. In order to provide a simple explanation of this result, let us analyze the time domain impulse response of the tunnel. The decrease of the power delay profile can be partly due to the increasing distance between each image of the transmitter and the receiver. However, the power decreases mainly because of the large number of reflections on the walls of images located far away from the tunnel axis. This is because most of the energy is guided inside the tunnel whose walls are imperfect conductors (i.e the reflection coefficient is less than one) and part of the energy is dissipated at each reflection. Therefore, as the distance between the transmitter and the receiver increases, so does the number of reflections and the amount of energy dissipated in the walls of the tunnels. Furthermore, a detailed analysis shows that the contribution of the rays reflecting many times on the horizontal walls are strongly attenuated because of the poor reflection coefficient associated with a vertical polarization. As a consequence, the shape of the channel impulse response is mainly determined by the images of the transmitter located in horizontal planes, either containing the transmitting antenna, or placed nearby.

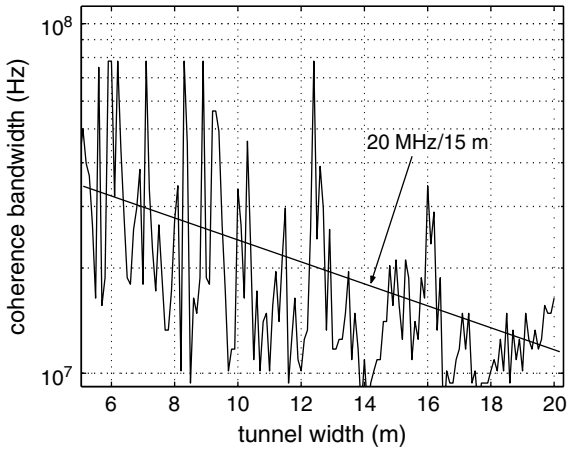

Fig. 2. Variation of the coherence bandwidth *versus* the tunnel width.

In order to simplify the calculation of the slope of the power delay profile, let us consider the contribution of the images situated in the plane containing the transmitting antenna centered in the tunnel. The two-dimensional geometry is represented in Figure 3. The transmitting and receiving points (Tx and Rx) are situated in a tunnel of width L at the points O and A, respectively. For large values of the distance x, we can assume that $x \gg mL$, where mL is the transverse distance between the mth image and the transmitter. The reflection coefficient R_{TE} associated with the TE polarization on the vertical walls is given by

$$R_{TE} = \frac{\sin\alpha - \sqrt{n^2 - \cos^2\alpha}}{\sin\alpha + \sqrt{n^2 - \cos^2\alpha}} \tag{5}$$

where n is the relative refractive index of the walls. Since, at high frequencies, the inequality $\sigma \gg \omega\varepsilon_r$ holds, and assuming that the distance between the transmitter and the receiver is large enough so that only rays impinging the walls with a grazing angle of incidence ($\alpha \ll 1$) play a leading part in the propagation, Equation (5) can be rewritten as

$$R_{TE} = \frac{\alpha - k}{\alpha + k} \tag{6}$$

where $k = \sqrt{\varepsilon_r - 1}$. As α is much smaller than k, an approximate expression of R_{TE} can be obtained as follows:

$$R_{TE} \approx -(1 - 2\alpha/k) \tag{7}$$

The mth ray reflects m times on the vertical walls. Its attenuation $a^{(m)}$, expressed in dB and referred to the

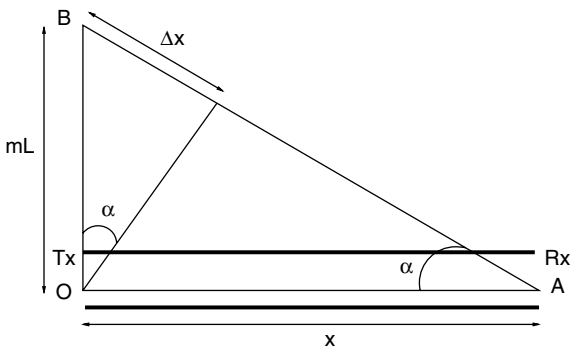

Fig. 3. Geometrical configuration in a horizontal plane.

direct ray, is deduced from Equation (7) and from the following trigonometric relations in Figure 3

$$\tan\alpha \approx \alpha \approx \frac{mL}{x} \approx \frac{\Delta x}{mL} \tag{8}$$

This leads to

$$a^{(m)} \approx \frac{40\ m^2 L}{kx} \approx \frac{40\Delta x}{kL} \tag{9}$$

Considering the relationship between the additional delay Δt of the mth ray and its additional path Δx, the decay of the power delay profile, expressed in dB per 100 ns, is given by

$$a^{(m)} \approx \frac{1200}{L\sqrt{\varepsilon_r - 1}} \mathrm{d}B/100\ ns \tag{10}$$

From Equation (10), it is apparent that the decay in dB is inversely proportional to the tunnel width, which will thus be a crucial parameter. A simple numerical particularization shows that, even for a tunnel 15 m wide, this slope reaches the value of 40 dB/100 ns. Taking into account that the duration of a GSM-R symbol is 3.7 μs, we deduce that the channel can be modeled as a single-tap flat-fading channel. Consequently, for this ideal geometrical configuration, only rays having a grazing angle of incidence on the tunnel walls play a leading part in the propagation and most of the energy propagates along the tunnel axis.

In real tunnel environments, distributed obstacles and variations in the tunnel shape give rise to a larger angular spread. In any case, however, it would be necessary to find a compromise between using directive antennas that increase the mean signal-to-noise ratio (SNR) and using omnidirectional antennas that allow a good exploitation of reflections on random obstacles. Indeed, one can imagine that the gain, which can be obtained with a multiple-antenna transmission and omnidirectional antennas, may also be obtained by only increasing the antenna gain of a single-antenna transmission. For the experimental measurements whose results are described in the next subsection, horn and patch antennas having a total beam width of about 90° have thus been chosen *a priori*. Nevertheless, additional measurements made with half-wave vertical dipoles have shown that the statistical properties of the MIMO channel were nearly identical.

3.2. Measurement Experiments and Data Processing

Experimental measurements of subway tunnel channels with multiple antennas have been carried out in the subway of Paris, at the station 'Porte des Lilas' in a tunnel presenting successively straight and slightly curved parts (*one way*) and in a tunnel exhibiting a large bend (*two way*). The experimental measurements setup consists of four fixed horn antennas placed on the station platform at a height of 2 m and four patch antennas placed behind the windscreen of the train. The complex impulse responses were measured with a channel sounder having a bandwidth of 35 MHz by switching the antennas successively. The measurements were taken stopping the train approximately each 2 m and taking about 1 second to measure and to store the 4×4 complex impulse responses. Since there is nobody on the platform or on the track, the channel remains stationary during each set of measurements.

Typical impulse responses in a *one-way* tunnel of the Paris subway are shown in Figure 4 for distances between the transmitting and the receiving antennas equal to 75 m and 350 m, respectively. For the smallest distance, the train is in the line of sight of the platform while, at 350 m, the train is situated after a bend that masks the transmitting antenna. The vertical axis of Figure 4 is on an arbitrary linear scale, while the horizontal scale is 200 ns div^{-1}. For GSM-R applications, it clearly appears that a single-tap model is sufficient to characterize the channel. This is in accordance with theoretical propagation modeling described before. Nevertheless, it must be emphasized that this result could be questionable in other situations in which the approximate translation symmetry is no longer valid, such as a *two way* tunnel in the presence of other trains.

Since the channel is flat-fading, each impulse response $h_{ji}(t)$, corresponding to the time domain channel characteristics between ith transmitting antenna and the jth receiving antenna, reduces to a complex number corresponding to the maximum value of the impulse response. One of the main problems to be solved before interpreting the data is to subtract the effect of the longitudinal attenuation. Indeed, in an indoor environment, for example, the movement of the mobile occurs in a small area, and we can assume that the mean value of the electric field remains a constant. In a tunnel, however, the longitudinal attenuation is very important, on the order of or greater than 10 dB/100 m. Since we are interested in the improvement brought by spatial diversity techniques for a given mean value of the SNR, the path loss must be subtracted. For straight tunnels, both theoretical results and experimental measurements in the frequency domain have shown

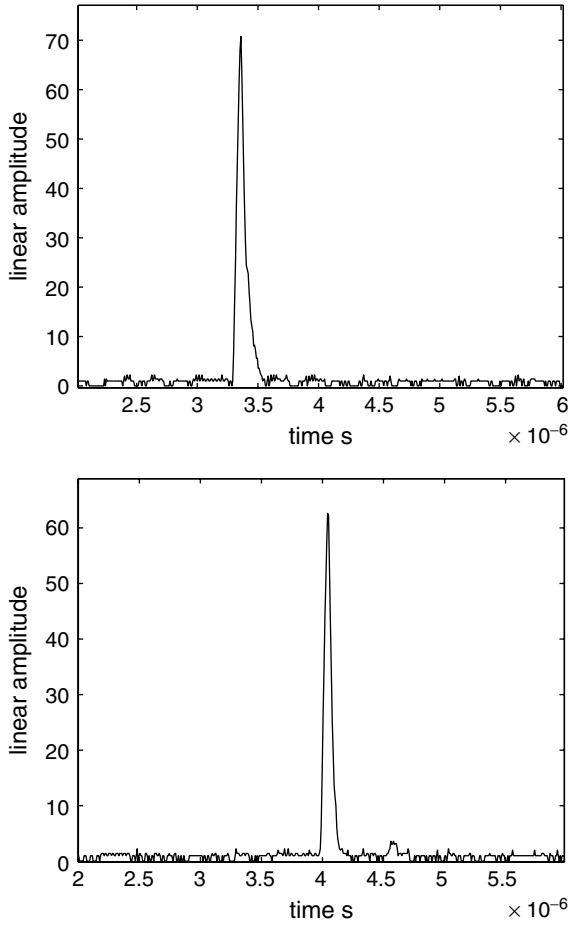

Fig. 4. Typical impulse responses in a one-way tunnel for two distances between the fixed and mobile antennas: (a) 75 m and (b) 350 m.

that the tunnel length can be divided into various intervals or 'zones' so that the mean value of the field exhibits an exponential decrease (therefore linear in dB) *versus* distance inside each zone. To remove the mean path loss, the statistical analysis is thus usually made on the basis of field fluctuations around the regression lines in the various zones of the tunnel [20].

In the Paris subway, where the measurements are performed, there is a succession of curves, straight parts and various changes of the tunnel cross section. In spite of this, however, a one-slope model conveniently fits the mean decrease of the field amplitude for each set of measurements that correspond to a length of about 200 m. The preliminary data processing is thus the following: store the **H** matrix for successive positions every 2 m; compute the average power of each matrix and then the regression line of the variation of the average power *versus* distance and finally, normalize the amplitude of each element h_{ji} around the square root of the value that the regression line takes at that position.

3.3. Capacity Analysis

Many trials have been performed to find out the optimum position of the antennas inside each array, looking for minimizing the spatial correlation between the various paths and always taking into account the operational constraints. It is apparent that the patch antennas at reception must be placed as far as possible and this is accomplished when locating the patches at each corner of the windscreen of the train. Again, at a first glance it seems that the transmit horn antennas should be positioned perpendicular to the track since this configuration yields to larger spatial diversity. Because of the platform width, the maximum space between the horn antennas is 1 m, that is, 3λ. In order to validate this statement about the position of the transmit horn antennas, we will also show the obtained results for a different configuration in which the horn antennas are placed parallel to the track.

From the sets of measured **H** matrices, the capacity of a given MIMO channel, C, can be calculated as [1]

$$C = \log_2 \det\left(\mathbf{I}_{L\times L} + \frac{\mathrm{SNR}}{N}\mathbf{H}\mathbf{H}^{\mathrm{H}}\right) \text{ bps/Hz} \qquad (11)$$

where SNR is the average signal-to-noise ratio per receiving antenna, $\mathbf{I}_{L\times L}$ is the $L \times L$ identity matrix, N is the number of transmitting antennas and the upper script$^{\mathrm{H}}$ means transpose conjugate (Hermitian).

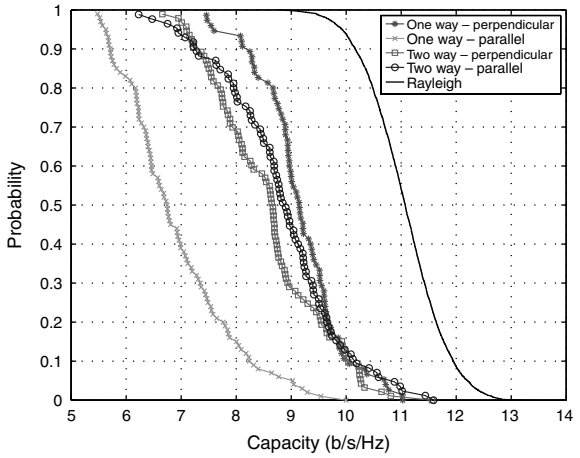

Fig. 5. Complementary cumulative distribution function of the channel capacity calculated for various shapes of the tunnel (4×4 antennas). Comparison with the case of i.i.d. Rayleigh channels.

The complementary cumulative distribution function of the capacity is given in Figure 5 for the previous configurations, by assuming a mean SNR of 10 dB. For comparison purposes, Figures 6 and 7 show, respectively, the capacity for a 2×2 antennas system (obtained by picking up the coefficients of the channel matrix corresponding to the most separated antennas) and for an 1×1 antennas system. It is apparent that channel capacity increases with the number of antennas. For instance, considering an outage probability of 0.5 and the *one-way-parallel* configuration, the channel capacities for the 4×4, 2×2 and 1×1 antennas cases are, respectively, 6.7, 4.6 and 3 (b s^{-1} Hz^{-1}). Note also that for the other configurations the capacity gains obtained by increasing the number of antennas are greater.

It is interesting to note that the *one-way-parallel* configuration has the maximum capacity in the 1×1 case, while it has the poorest capacity in the 2×2 and 4×4 antennas cases. This is due to the presence of high correlations between the coefficients of the channel matrix. Figure 8 shows the observed correlation between the first coefficient, h_{11}, and the other coefficients of the channel matrix for the *one-way* configurations. It is clear that the *one-way-parallel* configuration exhibits a higher spatial correlation than the *one-way-perpendicular* configuration. Similar conclusions were obtained when making comparisons between other configurations.

From the above explanations, we conclude that when considering tunnels that present large bends (*two way*), the position of the transmit antennas is not important since spatial diversity is introduced by the channel bend. On the other hand, the position of the transmit antennas is crucial for straight tunnels (*one way*). In this case, measurements reveal that placing the antennas perpendicular to the track is the best choice.

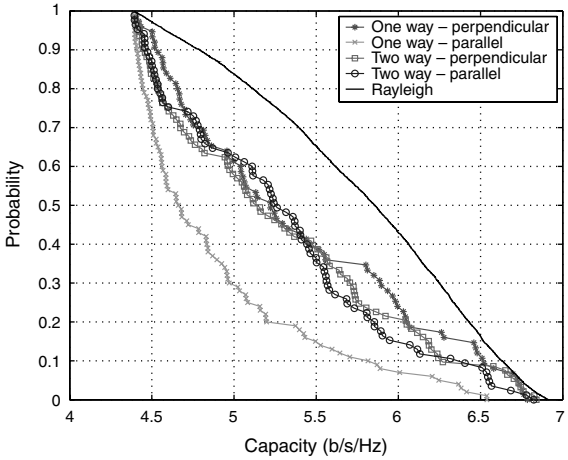

Fig. 6. Complementary cumulative distribution function of the channel capacity calculated for various shapes of the tunnel (2×2 antennas). Comparison with the case of i.i.d. Rayleigh channels.

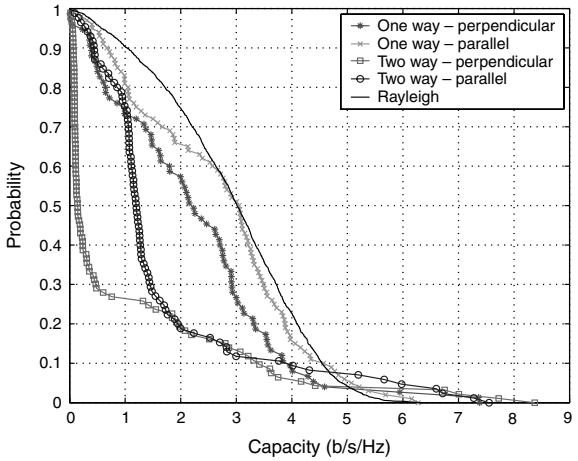

Fig. 7. Complementary cumulative distribution function of the channel capacity calculated for various shapes of the tunnel (1×1 antennas). Comparison with the case of i.i.d. Rayleigh channels.

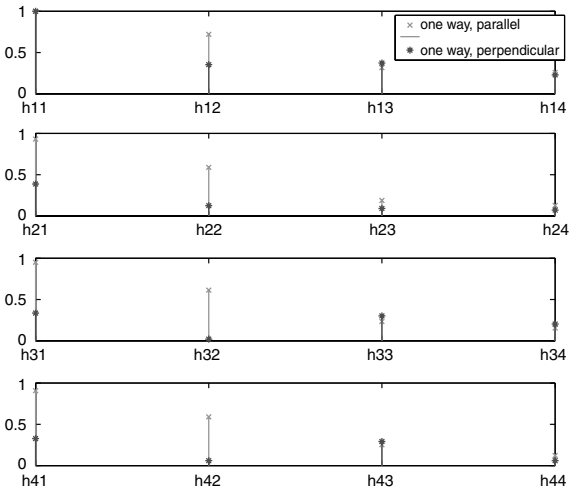

Fig. 8. Spatial correlations between coefficients of the channel matrix.

4. Space—time Equalization

In this section we address the problem of compensating the effect of both the noise and the controlled ISI induced by the GMSK modulation format. Mathematically speaking, this problem is equivalent to

detecting uncoded data that are mutually independent in both temporal and spatial dimensions. The first considered approach is the Space–Time Maximum-Likelihood (STML) equalizer [21]. If all input message sequences are equally likely, it is well known from information theory that the equalizing strategy that achieves the minimum probability of error is the one that chooses the transmitted message that maximizes the conditional probabilities known as likelihood functions.

In order to formulate the STML equalizer, let us rewrite the observations vector given by Equation (4) in a different way

$$\mathbf{x}(n) = \underline{\mathbf{H}}\,\underline{\mathbf{b}}(n) + \mathbf{g}(n) \tag{12}$$

where

$$\underline{\mathbf{H}} = [\mathbf{H}\, f(m-1) \quad \mathbf{H}\, f(m-2) \quad \cdots \quad \mathbf{H}\, f(0)] \tag{13}$$

is the channel matrix, with dimensions $Nm \times L$. Recall that m is the memory of the modulation ($m = 3$ in GSM) and $f(l)$ is the equivalent discrete-time impulse response. The term $\underline{\mathbf{b}}(n)$ in Equation (12) is the set of transmitted symbols that take part in the n-th vector of observations and is given by $\underline{\mathbf{b}}(n) = [\mathbf{b}^{\mathrm{T}}(n-m+1)\ \mathbf{b}^{\mathrm{T}}(n-m+2)\ \cdots\ \mathbf{b}^{\mathrm{T}}(n)]^{\mathrm{T}}$ and $\mathbf{g}(n) = [g_1(n), \ldots, g_L(n)]^{\mathrm{T}}$ is a vector of white Gaussian random processes that represents the noise.

It is well known that for a Gaussian channel and equiprobable transmitted symbols, the ML criterion is equivalent to minimizing the Euclidean distance between the transmitted and the received symbols. Having in mind the definition of $\mathbf{x}(n)$ given by Equation (12), the ML criterion consists of choosing the transmitted sequence $\mathbf{b}(0\colon K-1) = [\mathbf{b}^{\mathrm{T}}(0)\cdots\mathbf{b}^{\mathrm{T}}(K-1)]^{\mathrm{T}}$ that minimizes the following Euclidean distance

$$\hat{\mathbf{b}}(0\colon K-1) = \arg \min_{\mathbf{b}(0:K-1)} \times \left\{ \theta_{\mathrm{ML}}(\mathbf{b}(0\colon K-1)) = \sum_{n=0}^{K-1} \|\mathbf{x}(n) - \underline{\mathbf{H}}\,\underline{\mathbf{b}}(n)\|^2 \right\} \tag{14}$$

This optimization problem can be efficiently solved by means of a multistream Viterbi algorithm whose metric associated to each step is

$$\lambda_{\mathrm{ML}} = \|\mathbf{x}(n) - \underline{\mathbf{H}}\,\underline{\mathbf{b}}(n)\|^2 \tag{15}$$

Formulating the Viterbi algorithm requires a trellis representation of the ST modulator. The number of states at each trellis step is $2^{N(m-1)}$, and the number of branches that outputs from each state is 2^N. At the same time, the number of branches that arrive at each state is also 2^N. The Viterbi algorithm calculates the 2^N metrics associated with each of the $2^{N(m-1)}$ steps and retains the smallest values (survivors). Nevertheless, when using the Viterbi algorithm, complexity is proportional to $2^{N(m-1)}$, and thus, exponential in both the number of transmitting antennas and the memory of the modulation ($m = 3$ in GSM). When the number of antennas increases, the solution of Equation (14) becomes impractical.

Further complexity reduction can only be achieved at the expense of formulating suboptimum ST equalization algorithms. We have considered a Space–Time Linear Separation (STLS) equalizer that utilizes the receiver structure plotted in Figure 9. The objective of the linear filters is to spatially separate the transmitted signals in a way that each output extracts a single signal, that is,

$$\mathbf{y}(n) = \mathbf{W}^H \mathbf{x}(n) = \mathbf{W}^H \mathbf{H}\mathbf{s}(n) + \mathbf{r}(n) \tag{16}$$

where $\mathbf{r}(n) = \mathbf{W}^H \mathbf{g}(n)$ is the Gaussian noise at the output of the linear filters. The source signals are separated when each output corresponds to a single and different signal, that is, when $\mathbf{W}^H\mathbf{H} \approx \mathbf{I}_{N\times N}$. In this case, $y_i(n) \approx s_i(n) + r_i(n)$, $i = 1, \ldots, N$ and the Maximum-Likelihood estimation of the GMSK symbols $b_i(0\colon K-1)$ can be carried out by solving the following optimization problem

$$\hat{b}_{i,\mathrm{ML}}(0\colon K-1) = \arg \min_{b_i(0:K-1)} \left\{ \Theta_{i,\mathrm{ML}}(b_i(0\colon K-1)) = \sum_{n=0}^{K-1} \|y_i(n) - s_i(n)\|^2 \right\}$$

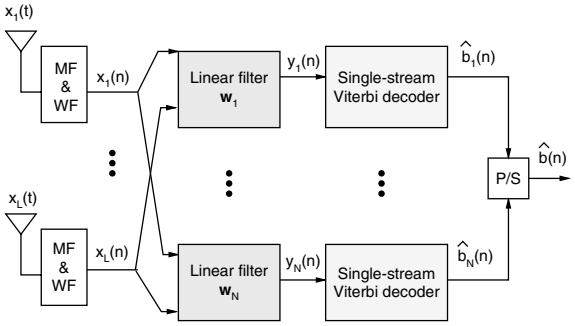

Fig. 9. Space–Time Linear Separation (STLS) equalizer structure.

$$= \arg \min_{b_i(0:K-1)} \left\{ \Theta_{i,\mathrm{ML}}(b_i(0:K-1)) \right.$$

$$\left. = \sum_{n=0}^{K-1} \| y_i(n) - \sum_{l=0}^{m-1} f(l) b_i(n-l) \|^2 \right\} \quad (17)$$

that can be efficiently solved using a single-stream Viterbi algorithm. Note that the complexity of the STLS structure, although exponential with the modulation memory, grows linearly with the number of transmitting antennas.

Different criteria can be used to select the coefficients of the linear separating system [21, 4]. The Minimum Mean Square Error (MMSE) criterion is the most reasonable choice since it leads to a compromise between signal separation and noise amplification. It is well known that the weight vectors that minimize the MSE between $\mathbf{y}(n) = \mathbf{W}^H \mathbf{x}(n)$ and $\mathbf{s}(n)$ are given by the Wiener solution

$$\mathbf{W}_{\mathrm{MMSE}} = \mathbf{R_x}^{-1}\mathbf{P} = (\sigma_s^2 0 \mathbf{H}\mathbf{H}^H + \sigma_g^2 \mathbf{I}_{L\times L})^{-1}\mathbf{H} \quad (18)$$

where $\mathbf{R_x} = E[\mathbf{x}(n)\mathbf{x}^H(n)] = \sigma_s^2 \mathbf{H}\mathbf{H}^H + \sigma_g^2 \mathbf{I}_{L\times L}$ is the autocorrelation matrix of the observations and $\mathbf{P} = E[\mathbf{x}(n)\mathbf{s}^H(n)] = \mathbf{H}$. The signal power and noise power are represented by σ_s^2 and σ_g^2, respectively. In the above solution, we have assumed that both the channel matrix and the signal and noise power are known. In practice, the Wiener solution can be estimated using the training sequence included in the GSM frames using conventional adaptive algorithms [22].

The performance of the previous ST equalizer can be considerably improved at the expense of little complexity increase, if the equalizer structure with linear cancellers shown in Figure 10 is employed [21]. We will use the term Space–Time Successive Cancellation (STSC) to denote this equalizer. The basic idea is to use a linear filter followed by a single- stream Viterbi equalizer to initially demodulate one of the transmitted data streams. The detected symbols are then used to reconstruct the transmitted signal to eliminate it from the received vector and to obtain a new input with fewer components. This new input is now used to demodulate a second data stream that is again remodulated and subtracted from the input. This deflation process is repeated consecutively until all the transmitted streams have been detected. As before, note that the complexity of this ST equalizer grows linearly with the number of transmitting antennas

Again, we have chosen the MMSE criterion to select the coefficients of the linear filters, that is,

$$\mathbf{w}_i = \left(\sum_{j=i}^{N} \sigma_s^2 \mathbf{h}_j \mathbf{h}_j^H + \sigma_g^2 \mathbf{I}_{L\times L} \right)^{-1} \mathbf{h}_i, \; i = 1, \ldots, N \quad (19)$$

where $\mathbf{w}_i$ are the coefficients of the i-th linear filter and $\mathbf{h}_i$ represents the ith column of the channel

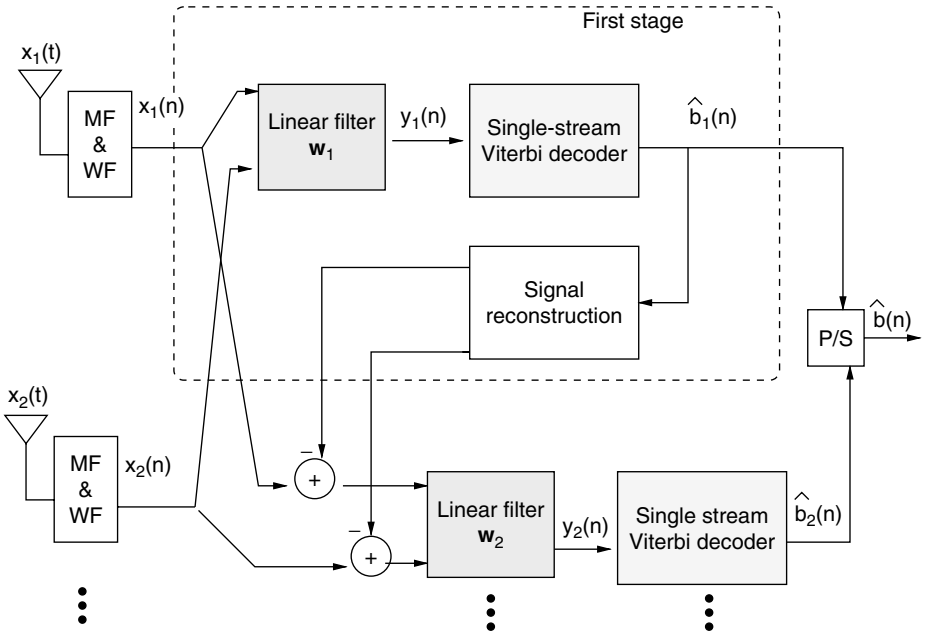

Fig. 10. Space–Time Successive Cancellation (STSC) equalizer structure.

matrix $\mathbf{H}$. The next step is to estimate the transmitted sequence $b_i(0{:}\,K-1)$ from the output of each linear filter

$$y_i(n) = \mathbf{w}_i^H \mathbf{x}_i(n) \approx s_i(n) + r_i(n),\ i = 1, \ldots, N \tag{20}$$

using a Viterbi equalizer. As mentioned above, the advantages of the STSC equalizer rely on the remodulation of the detected bits at each stage and the subtraction of the resulting signal, that is, the successive inputs are iteratively obtained as

$$\mathbf{x}_{i+1}(n) = \mathbf{x}_i(n) - \left(\sum_{l=0}^{m-1} f(l)\hat{b}_i(n-l) \right) \mathbf{h}_i \tag{21}$$

4.1. Computer Simulations

Computer simulations were carried out to illustrate the performance of the previously described ST equalizers for a 4×4 antennas system. We only focus on this number of antennas because significant gains in capacity are obtained with respect to a system with fewer transmitting and/or receiving antennas, as shown in Section 3. Figures 11, 12 and 13 plot the Bit-Error-Rate (BER) *versus* the Signal-to-Noise-Ratio (SNR) achieved with the STML, STSC and STLS space–time equalizers. The strong differences that exist between the equalizing methods are clearly seen: STLS is the worst method, STSC provides a gain with respect to STLS and STML is the best. Note that for an uncorrelated Rayleigh channel the difference in performance of the methods is much smaller. Also, it is interesting to observe that the configuration with worst performance is the *one-way-parallel*, which also exhibited the smaller channel capacity (see Section 3). The obtained results are in accordance with the fact that linear equalizers and decision feedback equalizers in single sensor systems severely degrade their performance when channels have bad spectral characteristics [15].

5. Space—time Decoding Receivers

This section deals with receivers that take into account the existence of a convolutional space–time encoder at transmission (see Figure 1). We can interpret the transmitter as the serial concatenation of the ST convolutional encoder and the GMSK modulator. The optimum receiving strategy is to perform the Maximum-Likelihood (ML) detection of the original information bearing sequence, $u(n)$, from the observations, $\mathbf{x}(n)$. This can be accomplished by means

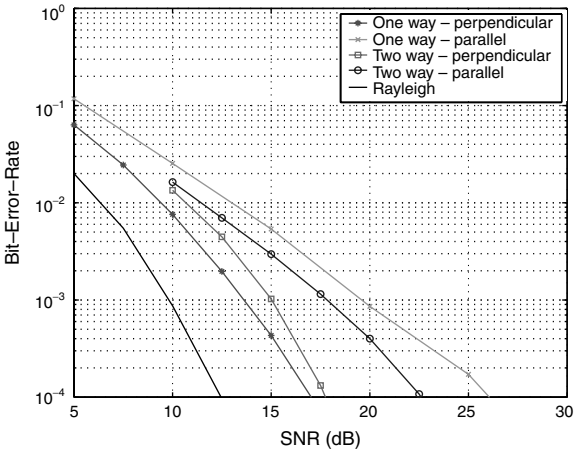

Fig. 11. Performance results for the STML equalizer.

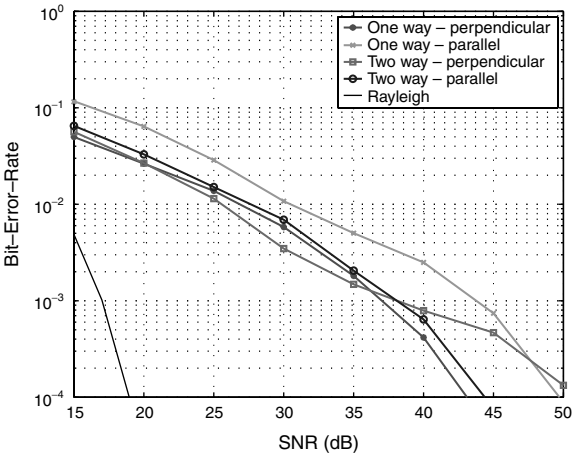

Fig. 12. Performance results for the STLS equalizer.

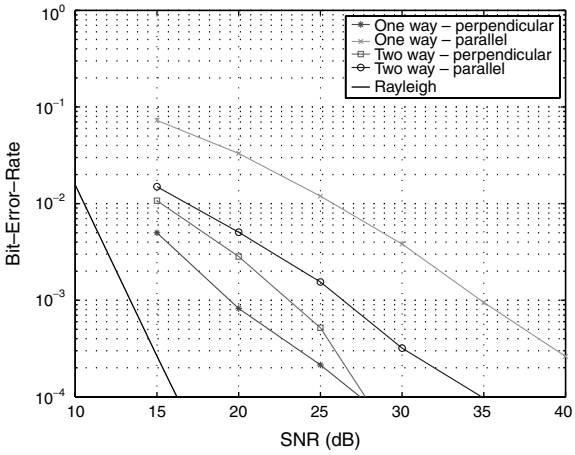

Fig. 13. Performance results for the STSC equalizer.

of a Viterbi algorithm that considers the *supertrellis* resulting from the combination of the trellises of the convolutional encoder and the GMSK modulator. The states of this *supertrellis* take the form (s_c, s_m) where s_c is a state belonging to the convolutional encoder trellis, and s_m is a state belonging to the GMSK modulator trellis. The *supertrellis* has $S_c \times S_m$ states, where S_c is the number of states of the convolutional encoder trellis, and $S_m = 4^N$ is the number of states of the GMSK modulator trellis, as explained in Section 4. To give an idea of how large this number can be, for an ST convolutional encoder of $S_c = 64$ states and $N = 4$ transmitting antennas, the number of states of the *supertrellis* is $S_c \times S_m = 16384$.

In order to avoid the above limitations, we will insert an interleaver between the ST encoder and the GMSK modulators to decouple both stages, and we will consider two suboptimal detection strategies. The first one simply consists of the concatenation of the STML equalizer described in the previous section with a Viterbi ML decoder. Hard decisions are passed from the equalizer to the decoder and there is no feedback from the decoder to the equalizer.

The second approach, shown in Figure 14, will be termed the iterative *Maximum A Posteriori* (MAP) decoding scheme. The equalizer and the decoder stages are more properly coupled in the sense that soft decisions are interchanged between the equalizer and the decoder in an iterative fashion. The key aspect in this strategy is that *all* the information about the symbols $\mathbf{b}(n)$ that the equalizer extracts from the observations $\mathbf{x}(n)$ is passed to the decoder. Note that in the previous scheme hard decisions are made (with a significant loss of information) before passing the information to the decoder.

From a statistical point of view, the best information about the coded bits $\mathbf{b}(n)$ that the equalizer can produce after observing $\mathbf{x}(n)$ are their *a posteriori* probabilities, that is, the probabilities of $\mathbf{b}(n)$ conditioned to the observed data $\mathbf{x}(n)$. These probabilities can be obtained by means of the Bahl-Cocke-Jelinek-Raviv (BCJR) algorithm. A more general form of this algorithm that considers, among other things, not only the computation of the *a posteriori* probabilities of the source bits but also the computation of the *a posteriori* probabilities of the coded bits is presented in References [23,24] and this is the version that we have used in this work. The work in References [23,24] refers to scalar valued sources and scalar coded symbols, but it can be easily extended to the vector case since no assumption is made about the symbol alphabet.

Let us start by denoting $P[\mathbf{b}(n); I]$ to the *a priori* probability of $\mathbf{b}(n)$, $P[\mathbf{s}(n); I]$ to the *a priori* probability of $\mathbf{s}(n)$, $P[\mathbf{b}(n); O]$ to the *a posteriori* probability of $\mathbf{b}(n)$ and $P[\mathbf{s}(n); O]$ to the *a posteriori* probability of $\mathbf{s}(n)$. The *a priori* probabilities and the *a posteriori* probabilities are the inputs and the outputs, respectively, of the algorithm. Taking the logarithm on all the probabilities

$$\begin{aligned} \pi[\mathbf{b}(n); I] &\equiv \log P[\mathbf{b}(n); I] \\ \pi[\mathbf{s}(n); I] &\equiv \log P[\mathbf{s}(n); I] \\ \pi[\mathbf{b}(n); O] &\equiv \log P[\mathbf{b}(n); O] \\ \pi[\mathbf{s}(n); O] &\equiv \log P[\mathbf{s}(n); O] \end{aligned} \tag{22}$$

the algorithm adopts a desirable additive form.

The iterative MAP decoding algorithm works as follows: Let e be an edge of the trellis with the following quantities associated: the starting state $s^S(e)$, the ending state $s^E(e)$, the input symbol $\mathbf{b}(n, e)$ and the output symbol $\mathbf{s}(n, e)$. The trellis is assumed to have a unique initial state S_0 and is assumed to finish in a unique ending state S_{K+m-1} where m is the memory corresponding to channel ISI. In order to

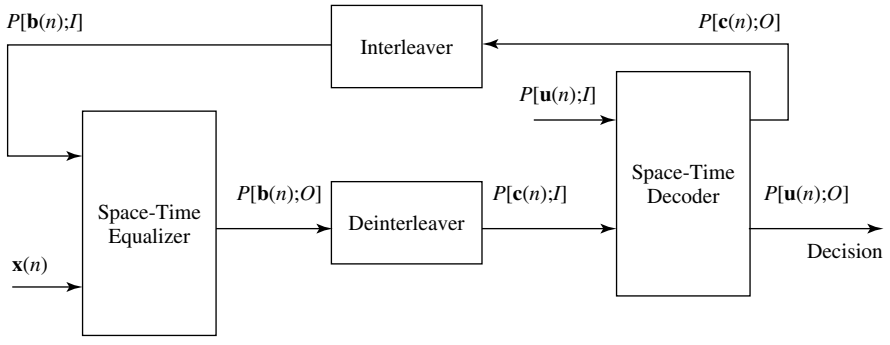

Fig. 14. Block Diagram of an iterative space–time decoder.

compute $\pi[\mathbf{b}(n); O]$ the algorithm performs the following recursions:

(1) *Forward recursion*

$$\alpha_n(s) = \log\left[\sum_{e:s^{\mathrm{E}}(e)=s} \exp\{\alpha_{n-1}[s^{\mathrm{S}}(e)] + \pi[\mathbf{b}(n,e); I] + \pi[\mathbf{s}(n,e); I]\}\right] \quad n = 1, \ldots, K+m \tag{23}$$

(2) *Backward recursion*

$$\beta_n(s) = \log\left[\sum_{e:s^{\mathrm{S}}(e)=s} \exp\{\beta_{n+1}[s^{\mathrm{E}}(e)] + \pi[\mathbf{b}(n+1,e); I] + \pi[\mathbf{s}(n+1,e); I]\}\right] \quad n = K+m-1, \ldots, 0 \tag{24}$$

$$\pi[\mathbf{b}(n); O] = \log\left[\sum_{e:\mathbf{b}(n,e)=\mathbf{b}(n)} \exp\{\alpha_{n-1}[s^{\mathrm{S}}(e)] + \pi[\mathbf{b}(n,e); I] + \beta_n[s^{\mathrm{E}}(e)]\}\right] + h_b \tag{25}$$

where

$$\alpha_0(s) = \begin{cases} 0 & s = S_0 \\ -\infty & \text{otherwise} \end{cases} \tag{26}$$

$$\beta_{K+m}(s) = \begin{cases} 0 & s = S_{k+m} \\ -\infty & \text{otherwise} \end{cases} \tag{27}$$

are the initial values for the recursions and h_b is the constant that makes $P[\mathbf{b}(n); O]$ a probability density function, that is,

$$\sum_{\mathbf{b}(n)} P[\mathbf{b}(n); O] = 1 \tag{28}$$

In the first iteration of the decoding process, it is assumed that the *a priori* probabilities of the information symbols, $P[\mathbf{b}(n); I]$ are uniform densities. The other input to the algorithm, $P[\mathbf{s}(n); I]$ is equal to the conditioned density of $\mathbf{s}(n)$ to the observations $\mathbf{x}(n)$, that is, $P[\mathbf{s}(n)|\mathbf{x}(n)]$.

Once computed in this way, the *a posteriori* probabilities are passed to the decoder. A deinterleaver is used in order to feed this set of *a posteriori* probabilities into the decoder in the same order that the coded symbols were emitted. Then the decoder uses these probabilities as *a priori* probabilities of the coded symbols, $P[\mathbf{c}(n); I]$, to compute the *a posteriori* probabilities of the original symbols assuming that the corresponding *a priori* probabilities, $P[u(n); I]$, are uniformly valued. Note that the algorithm for the decoding stage is the same as that for the equalizing stage described below, taking into account only the trellis of the convolutional code instead of the trellis of the GMSK modulator. Finally, a decision is made just choosing the original symbol with the higher *a posteriori* probability of having been transmitted

$$\hat{u}(n) = \arg\max_{u} P[u(n); O] \tag{29}$$

Up to this moment the only (although important) difference between this scheme and the ML approach described as our first suboptimal scheme is the usage of soft-valued decisions (i.e. the *a posteriori* probabilities) between the equalizer and the decoder. However, more refined decisions can be obtained if the decoder also computes the *a posteriori* probabilities of the coded symbols, $P[\mathbf{c}(n); O]$, and feeds them back into the equalizer as the *a priori* probabilities of the modulator input symbols, $P[\mathbf{b}(n); O]$. The computation of the *a posteriori* probabilities of the coded symbols can be made at the same point in the algorithm in which the *a posteriori* probabilities of the original symbols are computed, and through a similar expression given by

$$\pi[\mathbf{c}(n); O] = \log\left[\sum_{e:\mathbf{c}(n)(e)=\mathbf{b}(n)} \exp\{\alpha_{n-1}[s^{\mathrm{S}}(e)] + \pi[\mathbf{u}(n,e); I] + \beta_n[s^{\mathrm{E}}(e)]\}\right] + h_b \tag{30}$$

where $\mathbf{u}(n, e)$ is the input symbol associated with the trellis edge e. Note that these *a posteriori* probabilities must be interleaved to be properly fed back to the equalizer. The overall process is then repeated until no more improvement in symbol-error-rate is achieved.

Computer simulations were carried out to illustrate the performance of the previously described receiving strategies. We considered the same communication system as in the previous section but with the ST full diversity binary code given by the generator matrix $\mathbf{G} = [52, 56, 66, 76]$ (in octal representation) [25]. Figure 15 shows the BER *versus* the

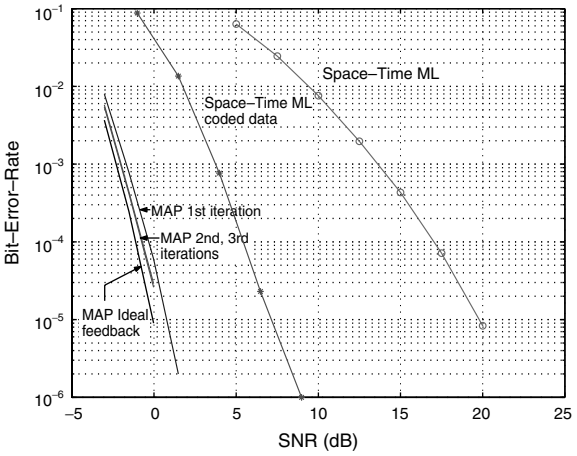

Fig. 15. Performance results for space–time decoding receivers.

SNR at the reception for the decoding schemes presented before, as well as for the STML uncoded system presented in Section 4, for comparison. Results were obtained for the *one-way-perpendicular* configuration. It can be seen that simply adding an ST encoder and performing ML decoding improves the performance of the system (e.g. the required SNR to reach a BER of 10^{-4} diminishes in 12 dB). Also note that this improvement with respect to the STML, is higher when MAP decoding is performed. For instance, it can be seen that in the first iteration an 18-dB gain in SNR is obtained for a BER of 10^{-4}. Nevertheless, no significant improvement has been obtained when performing more iterations. Some reasons explaining why the GMSK modulation format does not present improvement through iterations are given in Reference [26]. This phenomenon, however, does not mean that the iterative scheme does not work: we have also included in Figure 15 the BER obtained by an ideal MAP decoder, that is, the one that permits to feed into the equalizer the true *a priori* probabilities of the modulator input symbols. Note that there exists no significant difference between the curve corresponding to the ideal MAP decoder and the curves obtained after the second and third iterations. This means that, even when we have perfect knowledge of the symbols that were fed into the GMSK modulator, the performance of the equalizing stage is not significantly better than the performance when the knowledge, in the form of *a priori* probabilities, is fed back from the decoder to the equalizer.

6. Conclusion

The improvement of GSM radio interfaces in subway tunnels by means of antenna arrays and ST receivers has been investigated. We have demonstrated, both theoretically and experimentally, how the wireless propagation in subway tunnels can be conveniently modeled as a flat-fading channel. Nevertheless, experiments revealed that there exist strong spatial correlations among channel components that reduce channel capacity and severely affect receivers' performance. Receivers comprising of an ST equalizer and an ST decoder have been considered. Three different ST equalization strategies have been described. STML equalization is the technique that exhibits the lowest BER and the largest robustness but presents the largest complexity. On the other hand, STLS and STSC are much less complex but their performance is considerably worse. Thus, the selection of one method or the other will depend on the trade-off between complexity and performance that the receiver designer wishes to reach. We have also analyzed the performance of receivers with ST coding capabilities. We have demonstrated that MAP receivers that interchange soft information among the equalization and the ST coding stages exhibit a much better performance than those ML receivers that deal with hard decisions. Because of the poor characteristics of the GMSK modulation employed in GSM systems, the most important improvement in performance is achieved after the first iteration of the MAP receiver. However, no more significant improvement is observed after the following iterations.

Acknowledgments

This work has been supported by the European Commission under contract number IST-1999-20006 (ESCORT project).

References

1. Telatar IE. Capacity of Multi-Antenna Gaussian Channels. Technical Memorandum, Bell Laboratories, Lucent Technologies, October 1995.
2. Raleigh GG, Cioffi JM. Spatio temporal coding for wireless communication. *IEEE Transactions on Communications* 1998; **46**(2): 357–366.
3. Foschini GJ, Gans MJ. On limits of wireless communications in a fading environment. *Wireless Communication Magazine* 1998; **6**: 311–335.
4. Paulraj A, Papadias CB. Space-time processing for wireless communications. *IEEE Signal Processing Magazine* 1997; **14**(6): 49–83.

5. Tarokh V, Seshadri N, Calderbank AR. Space-time codes for high data rate wireless Communication: performance criterion and code construction. *IEEE Transactions on Information Theory* 1998; **44**(2): 744–765.
6. Naguib AF, Seshadri N, Calderbank AR. Increasing data rate over wireless channels. *IEEE Signal Processing Magazine* 2000; **17**: 76–92.
7. Lozano A, Farrokhi F, Valenzuela R. Lifting the limits on high-speed wireless data access using antenna arrays. *IEEE Communications Magazine* 2001; **39**(2): 33–42.
8. Bauch G. Concatenation of space-time block codes and turbo-TCM. In *Proceedings of the IEEE International Conference on Communications*, Vol. 2, June 1999; pp. 1202–1206.
9. Lin X, Blum RS. Improved space-time codes using serial concatenation. *IEEE Communication Letters* 2000; **4**: 221–223.
10. Stefanov A, Duman TM. Turbo-coded modulation for systems with transmit and receive antenna diversity over block fading channels: system model, decoding approaches, and practical considerations. *IEEE Journal on Selected Areas in Communications* 2001; **19**(5): 958–968.
11. Liu Y, Fitz MP, Takeshita OY. Full rate space-time turbo codes. *IEEE Journal on Selected Areas in Communications* 2001; **19**(5): 969–980.
12. Shiu D, Foschini G, Gans M, Kahn J. Fading correlation and its effect on the capacity of multi-element antenna systems. *IEEE Transactions on Communications* 2000; **48**: 502–513.
13. D'Andrea AN, Mengali U. *Synchronization Techniques for Digital Receivers*. Plenum Press: New York, 1997.
14. Blahut R. *Digital Transmission of Information*. Addison-Wesley: Reading, MA, 1990.
15. Proakis JG. *Digital Communications*. McGraw-Hill: Singapore, 1995.
16. Chen SH, Jeng SK. SBR image approach for radio wave propagation in tunnels. *IEEE Transactions on Vehicular Technology* 1996; **45**(3): 570–578.
17. Didascalou D, Venot Y, Wiesbeck W. Modelling and measurement of EM-wave propagation in the Berlin subway. In *Proceedings of the AP 2000 International Symposium, Davos*, April 2000; p. 217–220.
18. Mahmoud SF, Wait JR. Geometrical optical approach for electromagnetic wave propagation in rectangular mine tunnels. *Radio Science* 1974; **9**: 1147–1158.
19. Hwang Y, Zhang YP, Kouyoumjian RG. Ray-optical prediction of radio-wave propagation in tunnel environments. *IEEE Transactions on Antennas and Propagation* 1998; **46**(9): 1328–1345.
20. Lienard M, Degauque P. Propagation in wide tunnels at 2 GHz: a statistical analysis. *IEEE Transactions on Vehicular Technology* 1998; **47**(4): 1322–1328.
21. Verdú S. *Multiuser Detection*. Cambridge University Press: New York, 1998.
22. Haykin S. *Adaptive Filter Theory*, 4th edition, Prentice Hall: New York, 2002.
23. Montorsi G, Pollara F, Benedetto S, Divsalar D. A soft-input soft-output APP module for iterative decoding of concatenated codes. *IEEE Communication Letters* 1997; **1**(1): 11–13.
24. Benedetto S, Divsalar D, Montorsi G, Pollara F. A Soft-Input Soft-Output Maximum A Posteriori (MAP) Module to Decode Parallel and Serial Concatenated Codes. TDA Progress Report 42-127, November 1996.
25. Roger Hammons Jr A, El Gamal H. On the theory of space-time codes for PSK modulation. *IEEE Transactions on Information Theory* 2000; **46**(2): 524–542.
26. Franz V. Turbo-Detection for GSM-Systems: Channel Estimation, Equalization and Decoding. Ph.D. thesis, University of Munich, Germany, March 2000; pp. 56–63.

